Supporting Information

Commercial kitchen operations produce a diverse range of gas-phase reactive nitrogen species

Leigh R. Crilley[1,a], Jenna C. Ditto[2,3,b], Melodie Lao[1], Zilin Zhou[2,c], Jonathan P.D. Abbatt[3], Arthur W.H. Chan[2,3], Trevor C. VandenBoer[1]

[1] Department of Chemistry, York University

[2] Department of Chemical Engineering and Applied Chemistry, University of Toronto

[3] Department of Chemistry, University of Toronto

[a] Now at: Atmospheric Services, WSP Australia, Brisbane

[b] Now at: Department of Energy, Environmental, and Chemical Engineering, Washington University in St. Louis

[c] Now at: Exposure and Biomonitoring Division, Environmental Health Science and Research Bureau, Health Canada

This supporting information contains 5 sections of text, three tables and 15 figures.

S1 Methods

S1.1 tN_r instrument calibration, QA/QC and maintenance

The NO_x analyser on the tN_r instrument was calibrated with a gas-calibration system and a standard gas cylinder of NO (4.88 ppmv in N_2 ±5%, Linde Canada Inc., Toronto, ON) prior to the measurements, as per manufacturer specifications. The observed readings of NO_x by the tN_r instrument were found to agree well with a second co-located chemiluminescent NO_x analyser. An intercompared linear regression for measurements by the two analyzers, while they were above the limit of detection has a slope of 0.96, indicating that the additional materials required for the tN_r inlet were not affecting the quality of temporal response or accuracy of the NO_x measurements. The Na_2CO_3 and H_3PO_3 annular denuders integrated into the inlet where changed every two days with ones freshly prepared. Their scrubbing efficacy was confirmed using known amounts of the target species HONO and NH_3 and confirmed to be greater than 95 % before and after each change. The tN_r oven conversion efficiency to NO_x was checked periodically throughout the campaign using the in-situ NH_3 calibration source and was observed to have a mean of 110±27% over the campaign. The observed levels of $N_{r,base}$ were found to agree well with co-located Ogawa NH_3 passive samplers measurements (Section S1.3) and suggest that the tN_r instrument was quantitatively measuring this well-established indoor basic N_r species. The uncertainty in the tN_r measurement was estimated to be 20%, driven by uncertainty in the catalytic conversion of N_r species like NH_3 to NO_x in the oven and quantities being determined by difference.

S1.2 PTR-MS calibration, QA/QC and data processing

Data were collected every 30-seconds but are presented here as 1-minute averages. Every 5 hours, the instrument was calibrated with ~10 ppb of select gases (listed below) and zeroed with VOC-free air generated using a heated catalyst acting as a combustion-based scrubber. During the campaign, the following subset of species were calibrated with a standard gas cylinder from Apel Reimer and mixing ratios used in this analysis: acetonitrile (C_2H_3N), acetone (C_3H_6O), acrylonitrile (C_3H_3N), benzene (C_6H_6), toluene (C_7H_8), o-xylene (C_8H_{10}), a-pinene ($C_{10}H_{16}$), and 1,3,5-trimethylbenzene (C_9H_{12}). We calibrated additional species post-campaign that included: pyrrole (C_4H_5N), propionamide (C_3H_7NO), triethylamine ($C_6H_{15}N$), acetic acid ($C_2H_4O_2$), heptadienal ($C_7H_{10}O$), and nonanal ($C_9H_{18}O$). These calibrations were performed by evaporating liquid standards in to dry zero air, following the method described by Liu et al.[1]. Finally, several species were calibrated post-campaign with a different Apel Reimer cylinder: ethanol (C_2H_6O), acrolein (C_3H_4O), D4 siloxane ($C_8H_{24}O_4Si_4$), and hexanal ($C_6H_{12}O$). We report our PTR-MS's sensitivities for each of these calibrated chemicals in our companion paper (Figure S2 in[2]).

Data were processed in Tofware Version 3.2.5, based in Igor Pro. Detailed data processing steps are described in Ditto et al.[2] Non-targeted peak lists were generated for ions between m/z 30-500. Chemical formulas were assigned for lower molecular weight ions in the m/z 30-250 range, if a proposed formula within 10 ppm of the detected mass existed and had reasonable ratios of carbon, hydrogen, oxygen, nitrogen, sulfur, and chlorine atoms for small molecules, and if the proposed formula was the only one within 10 ppm or was clearly a better fit than other possibilities in this range. If there was no clear top formula choice, no formula was assigned. This m/z range was selected for confident peak identification given the mass resolution of the PTR-

MS instrument. In post-processing, signals were background subtracted and any signals below the limits of detection for a given ion were removed.

We acknowledge that with our 6.6 m long inlet, some VOCs may experience delays driven by gas-wall partitioning along the length of the PFA tubing. We observed a wide range of predominantly volatile organic compounds and intermediate volatility organic compounds in our measurements, whose observed estimated saturation concentration ranged from 10^3 to 10^{10} µg/m^3 (calculated using the molecular formula based approach in[3]), with most nitrogen-containing ions described in this paper falling in the range of 10^5 to 10^8 µg/m^3. According to work by Deming et al.[4] and Pagonis et al.[5], this could lead to variable delay times within the inlet tubing, e.g., approximately 2 min/m to <0.02 min/m[5] for the saturation concentration range of most N-containing species here. In our prior work with this inlet we see rapid transfer for a number of VOCs from cooking to the VOCUS without evidence for systematic tubing delays. Over the course of the cooking events described here (lasting minutes to hours), average N-containing ion signals at the estimated saturation concentration range, even if susceptible to a time delay on the order of 0.1-13 minutes based on the delay rates above, will not dramatically change observed plume analysis results[2].

S1.3 Supporting instrument methodology

American Ecotech chemiluminescent NO_x (Mo-catalyst, EC9841), and UV-absorption O_3 analyzers (Serinus 10), passive samplers for gas-phase NH_3 and amines. Two measurements of CO_2 and air change rate (ACR) were made: one in the kitchen and the other from the exhaust duct in a mechanical room housing the dedicated exhaust system for the commercial kitchen.

The gas analyzers were operated at 1-minute time resolution throughout the campaign, using the shared inlet for the former and an identical, but independent inlet for the latter due to pressure drop restrictions, which also had a filter at the entry to prevent particle intrusion. Ogawa passive samplers with citric acid-coated reactive substrates were installed in the kitchen close to the sampling inlet for an intercomparison of measured gas-phase NH_3 and amines levels. Citric acid coatings are standardized for volatile atmospheric base sampling, particularly for NH_3 by monitoring networks such as the US EPA[6,7]. The passive samplers were deployed for two periods, 7-13 and 13-17 Sept, and were extracted in 18.2 MΩ·cm deionised water followed by ion chromatography separation and conductivity detection, with full details available in Salehpoor et al. [8].

Two measurements of CO_2 and air change rate (ACR) were made: one in the kitchen and the other from the exhaust duct in a mechanical room housing the dedicated exhaust system for the commercial kitchen. Here, flows from the individual range hoods were combined to be vented outdoors. The measurements of CO_2 were made by simple non-dispersive infrared absorption (K30, Sensair, CO_2 Meter, Ormond Beach, FL, USA). These CO_2 sensors were calibrated prior to the campaign and logged measurements at 1-minute intervals. The kitchen ACR was determined by recording current output on the exhaust fan controller via an Arduino datalogger. This exhaust fan controller provides an analog output of 4-20 milliamperes (mA) that corresponds to the active rotation rate, which spans 0-1750 rotations per minute (RPM). The accuracy of the fan controller signal output is ± 10 %, as specified by the manufacturer (AAHC-550-UH HVAC drive controller,

AAB Group). These observations were supported further by data logged through an automated control system (DCKV Cloud Panel, Ecoazur, Laser Controls Ltd., Brampton, ON) which also recorded temperature and steam/smoke detection through blue light sensors installed in the cooking area range hoods. Irradiance throughout the commercial kitchen was measured by a spectral radiometer (StellarNet Inc.) roughly at head height and ~2 m from the ceiling, which is most relevant to consider the exposure for occupants or to model the chemical reactivity in the space relevant to such exposure.

S1.4 Details of production rate of HONO from NO_2 box model

The surface uptake coefficient of NO_2 (γ_{NO2}) describes the reaction probability of gaseous NO_2 when colliding with an indoor surface (e.g. to produce HONO) and was calculated using E2 following prior approaches[9,10].

$$\gamma_{NO2} = \frac{4\,k_{rem,NO2}\,V}{v_{NO2}\,S} \quad \text{(E2)}$$

where V is the geometric room volume (m^3), ω_{NO2} is the thermal velocity of NO_2 at the average indoor temperature over the campaign (28.0 °C; m s^{-1}), S is the geometric indoor surface area (m^2), and $k_{rem,NO2}$ is the removal rate of gaseous NO_2 to surfaces (s^{-1}) after accounting for loss by air exchange. Continuous measurements of NO_2* from the second chemiluminescence analyzer were used to find times when a peak in NO_2 levels was observed to decay exponentially, indicative of an isolated plume being removed. Twenty-three such events were observed (Table S1) and an exponential fit was applied to the decay from the maximum level of NO_2 to calculate the time constant (τ) and corresponding removal rate ($k_{rem,NO2}$ = 1/ τ). An example event and the fit to the decrease in NO_2 levels is shown in Fig S1, demonstrating that its decay was slightly faster than ACR, as would be expected if there was additional loss via surface uptake. However, this was not the case for all 23 events, with only 6 events observed to have an NO_2 removalfaster than ACR because the plume removal was happening very quickly (ACR=20-40 hr^{-1}). The resulting uptake coefficients for NO_2, therefore, likely represent upper limit on this potential chemistry and we consider additional uncertainties in the discussion below.

The HONO production rate (P_{HONO}; molec cm^{-3} s^{-1}) from the heterogeneous hydrolysis of NO_2 on surfaces according to the mechanism of R1 was calculated using E3. Values of P_{HONO} calculated with this approach also represent the upper limit of HONO formation from NO_2 hydrolysis[9], as retention of HONO on surfaces as nitrite from this reaction, or other NO_2 heterogeneous losses having a lower HONO yield, are possible[11–14] .

$$P_{HONO} = 0.5 \times k_{rem,NO2} \times [NO_2] \quad \text{(E3)}$$

The loss rate of HONO via photolysis (L_{HONO}; molec cm^{-3} s^{-1}) was calculated using the photolysis rate (J_{HONO}; s^{-1}) determined from the spectral radiometer measurements [15].

$$L_{hv} = J_{HONO}[HONO] \quad \text{(E4)}$$

The other major loss process for HONO is removal by the ventilation system (L_{ACR}; molec cm^{-3} s^{-1}) and was calculated based on the ACR (s^{-1}).

$$L_{ACR} = ACR \times [HONO] \quad \text{(E5)}$$

Taken together, the production and loss terms were then used to approximate the HONO levels (E6) for comparison to observations. Where there is a difference between these known mechanisms and observations, the presence of other production and/or loss terms can be inferred.

$$[HONO]_{pred} = (P_{HONO} - (L_{hv} + L_{ACR}))\,dt \quad \text{(E6)}$$

where $[HONO]_{pred}$ represents the HONO generated in sum from E3 through E5. Consequently, in the absence of direct emissions or outdoor air bringing HONO indoors, and based on the current state of knowledge indoors, the difference between the measured and predicted HONO will be equivalent to the HONO originating from or deposited onto surfaces, which act as reservoirs ($[HONO]_{sur}$; E7).

$$[HONO]_{sur} = [HONO]_{meas} - [HONO]_{pred} \quad \text{(E7)}$$

Due to its inlet duty cycle time, the tNr instrument did not capture the dynamic trends of the HONO emitted in short pulses directly from gas stove fuel combustion in the kitchen[16] and so the assumed mechanism inferred from E7 as reversible surface partitioning, when using observations to drive this model, is likely to be true. Note that if other HONO production or loss mechanisms are able to establish equilibrium on timescales similar to the ACR, that these would be encapsulated in our $[HONO]_{sur}$ term. Consequently, the calculated $HONO_{sur}$ can be converted to a flux from the room surfaces (E8) into the overlying air within the kitchen.

$$\square\square\square\square_{sur\_flux} = \frac{[HONO]_{sur}}{\left(\frac{S}{V}\right)\cdot dt} \quad \text{(E8)}$$

where the $HONO_{sur\_flux}$ is the flux from the surface in molec cm^{-2} s^{-1}, and S/V the geometric surface area to volume ratio of the kitchen (0.032 cm^{-1}), which dictates the surface in contact with the air in which $[HONO]_{sur}$ in molec cm^{-3} was measured, at a time resolution (dt in s) of the observations. In sum, these combined equations allow for description of the chemistry governing the observed HONO levels in the commercial kitchen which can be compared to observations in other indoor environments, whether experimental or under normal use.

S1.5: Comparison of TMA measured by PTR-MS and passive samplers

The ambient levels were below the co-deployed passive sampler detection limits for TEA (LOD = 2.59 ppbv for 5 days of collection), while the PTR-MS detected it at levels above its detection limits (on average 25 pptv). This would therefore indicate that TEA comprised a minor part of $N_{r,base}$ as its quantitative conversion by the tN_r oven[16] would generate less than 100 pptv of signal, which is less than 2% of the total $N_{r,base}$. In contrast, the trimethylamine (TMA) levels measured by the passive samplers were a factor of 35 larger than TEA observed by the PTR-MS (1.45 ppbv of TMA and 25 pptv of TEA, respectively), but unfortunately TMA was not calibrated directly for the PTR-MS. A theoretical estimate using the proton transfer reaction rate constant methods in Sekimoto et al.[17] of the campaign-wide TMA mixing ratio observed by the PTR-MS was calculated by scaling the TEA sensitivity down by 20% to account for the relative theoretical difference between the sensitivity of these two analytes. Note that this assumes that both compounds have the same degree of fragmentation in the PTR-MS ion-molecule reaction region, which is a reasonable estimate based on past measurements of both of these compounds with different instruments,

though TMA might fragment slightly less[5]. The resulting TMA mixing ratio from this sensitivity estimation is 0.28 ppb. This adjustment remains insufficient to resolve the difference between the passive sampler and PTR-MS observations. The difference remains substantial between the two techniques despite the passive sampler being within 2 m of the PTR-MS inlet and at approximately the same height. It is possible that a point source of TMA was located close to the passive samplers during this period, while the NH_3 measurements used for intercomparison to the $N_{r,base}$ represent kitchen-wide values. Also, there could be fragmentation of protonated TMA in the PTR-MS, which is not accounted for here. These issues make intercomparison of TMA and assessment of its role as a component of tN_r instrument measurements unexpectedly difficult.

Table S1. NO_2 decay events observed in the main kitchen during periods when the air exchange rate was stable.

Event	Background NO_2 (ppbv)	Peak NO_2 (ppbv)	τ (s)
1	13.9 ± 0.15	16.1 ± 0.65	279
2	12.1 ± 0.59	80.4 ± 2.8	777
3	20.6 ± 1.0	71.9 ± 4.5	148
4	19.8 ± 0.27	30.3 ± 1.0	79
5	6.5 ± 0.3	27.6 ± 0.55	418
6	17.6 ± 2.4	115.9 ± 7.6	136
7	13.6± 0.8	69.8 ± 3.8	123
8	8.9 ± 0.37	62.5 ± 2.1	171
9	7.6 ± 0.21	25.4 ± 0.65	240
10	8.5 ± 0.38	42.1 ± 1.1	53
11	9.2 ± 0.31	12.8 ± 0.82	130
12	11.8 ± 0.24	17.5 ± 0.8	160
13	11.7 ± 2.7	84.6 ± 3.5	389
14	15.4 ± 0.37	27.2 ± 1.8	78
15	7.8 ± 0.21	7.8 ± 0.59	345
16	12.8 ± 0.73	64.8 ± 2.1	62
17	10.7 ± 0.39	18.6 ± 1.1	73
18	8.9 ± 0.54	36.9 ± 2.2	40
19	9.6 ± 0.29	32.1 ± 1.3	313
20	7.9 ± 0.12	26.3 ± 0.5	483
21	15.1 ± 5.5	49.2 ± 5.9	163
22	19.0 ± 0.24	14.4 ± 0.84	124
23	7.7 ± 0.17	43.5 ± 1.1	152

Table S2. Model results from HONO production and loss calculations to infer surface source strengths, at hourly time resolution. The estimates range from a low to high role for NO_2 heterogeneous conversion (γ_{NO2}) with matching impacts from air change rates estimated at night (ACR_{night}) to provide upper and lower limits on the inversely-related level of importance for HONO surface sources. Number density equivalent values of the daily and nighttime only (22:00-06:00) contributions from the dominant terms are provided with one standard deviation in the hourly variability from the observations.

NO_2 Importance Scenario	Outcome Period	NO_2 to HONO Production (molec cm^{-3} hr^{-1})	HONO ACR Loss (molec cm^{-3} hr^{-1})	HONO from Surfaces (molec cm^{-3} hr^{-1})
Low ($\gamma_{NO2}=1x10^{-6}$; $ACR_{night}=1.0$)	Daily Average	$1.8\pm0.3 \times 10^{9}$	$1.9\pm1.4 \times 10^{10}$	$7.5\pm1.9 \times 10^{10}$
	Night Only	$1.8\pm0.1 \times 10^{9}$	$2.0\pm3.1 \times 10^{9}$	$5.6\pm0.3 \times 10^{10}$
Mid ($\gamma_{NO2}=2x10^{-6}$; $ACR_{night}=0.5$)	Daily Average	$3.5\pm0.6 \times 10^{9}$	$1.9\pm1.4 \times 10^{10}$	$7.3\pm1.9 \times 10^{10}$
	Night Only	$3.5\pm0.1 \times 10^{9}$	$1.6\pm3.2 \times 10^{9}$	$5.6\pm0.6 \times 10^{10}$
High ($\gamma_{NO2}=1.4x10^{-5}$; $ACR_{night}=0.$)	Daily Average	$2.5\pm0.5 \times 10^{10}$	$1.8\pm1.4 \times 10^{10}$	$5.3\pm1.9 \times 10^{10}$
	Night Only	$2.5\pm0.2 \times 10^{10}$	$1.3\pm3.3 \times 10^{9}$	$3.3\pm0.3 \times 10^{10}$

207 **Table S3.** Estimated surface emissions for calibrated VOCs from PTR-MS measurements.

Ion	µg hr $^{-1}$m^{-2}
NH_2CH^+	8.71E-01
$C_2H_3NH^+$	5.16E+00
$C_2H_6OH^+$	5.84E+02
$C_3H_3NH^+$	1.66E-01
$C_3H_4OH^+$	1.23E+01
$C_3H_6OH^+$	3.52E+01
$C_2H_4O_2H^+$	8.96E+01
$C_4H_5NH^+$	3.79E-01
$C_3H_7NOH^+$	5.90E+00
$C_6H_7^+$	3.86E+01
$C_7H_9^+$	1.61E+01
$C_6H_{12}OH^+$	7.88E+00
$C_6H_{15}NH^+$	3.55E-01
$C_8H_{11}^+$	1.05E+01
$C_7H_{10}OH^+$	2.82E+00
$C_9H_{13}^+$	4.16E+00
$C_{10}H_{17}^+$	1.20E+01
$C_9H_{18}OH^+$	1.18E+01
$C_{10}H_{30}O_5Si_5H^+$	3.54E+02

208

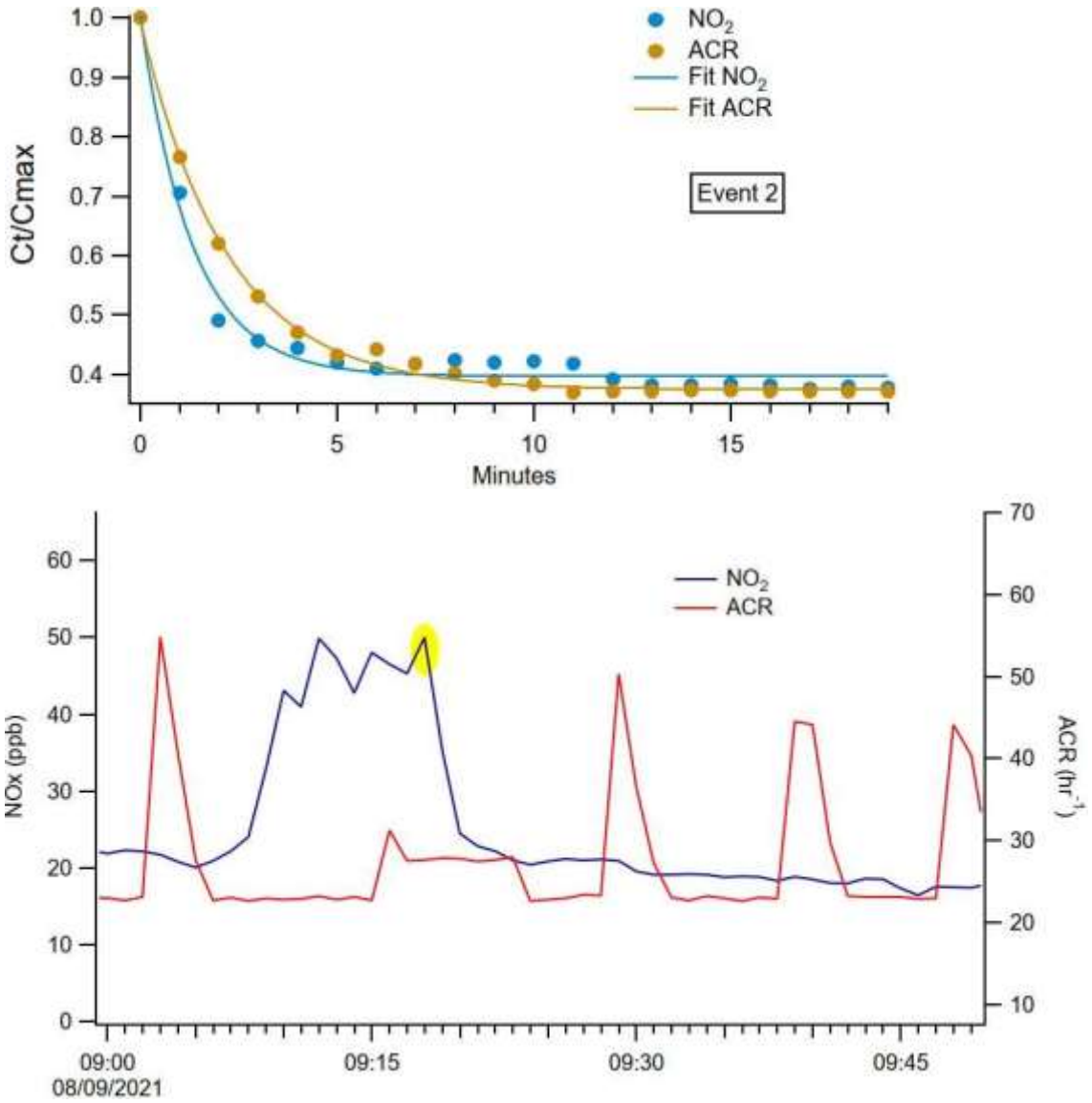

209

210

211 **Fig S1.** (Top) Normalised decay in NO_2 over time (blue circles) for a representative event starting
212 at ~9:20 AM in bottom panel (yellow highlighted circle around 9:20), equivalent to t = 0 minutes
213 here. The expected loss of NO_2 as calculated from the measured ACR alone (orange), which was
214 also fast, but slower than the observed NO_2 decay (blue). Note that NO_2 never decays to zero due
215 to a reservoir present in the kitchen. (Bottom) Time series of measured NO_2 mixing ratio and ACR
216 logged from the ventilation system for this event.

217

218

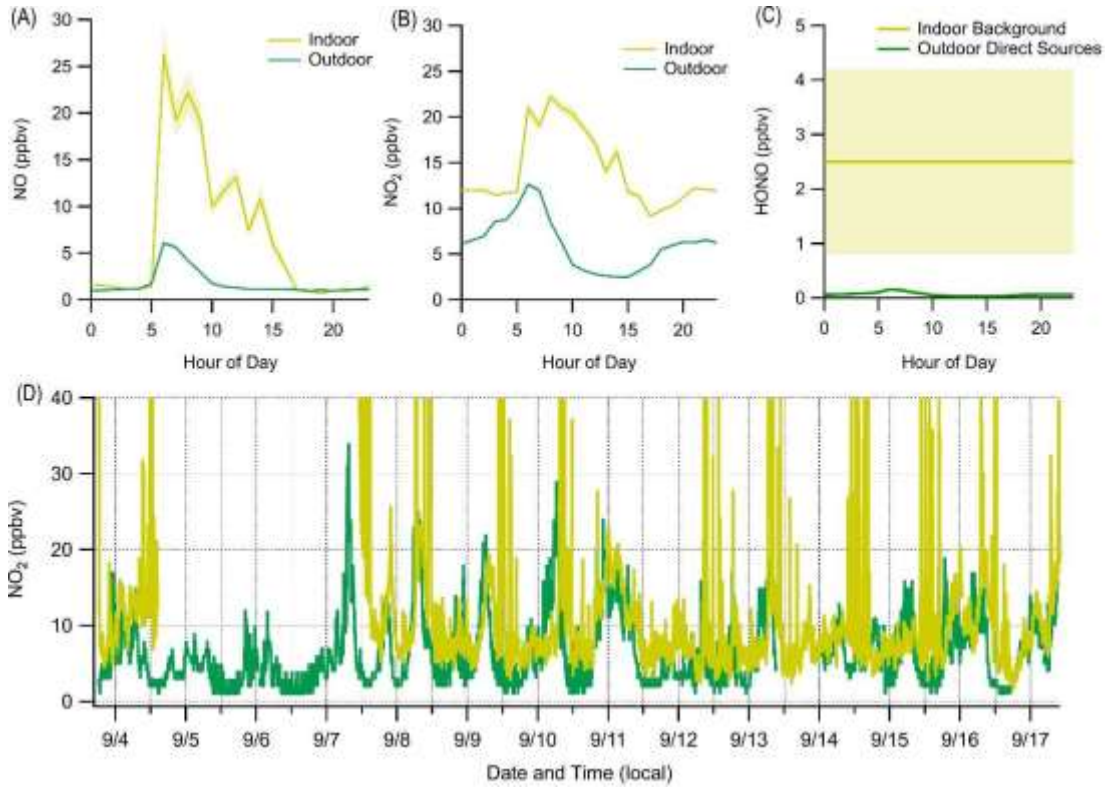

Fig S2: Diurnal averages of (A) NO and (B) NO_2 from within the kitchen (yellow) and the local Environment Canada – Downsview air quality monitoring station (green) during the KOCENA campaign. Shaded regions denote the standard error of the mean. (C) Mean HONO observed in the kitchen (error of one standard deviation) and estimated outdoor values based solely on a HONO/NOx emission ratio of 0.85% recently observed from a UK road tunnel[18]. The indoor kitchen time series of NO_2 (D) was often elevated at different times of day (axis limited to 40 ppbv; see Figure 1 for full range) compared to outdoors, especially during cooking.

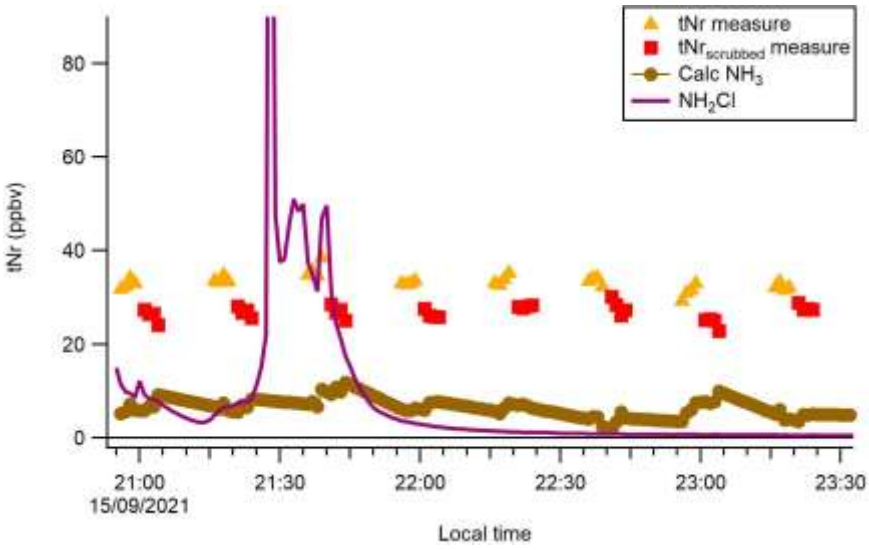

Fig S3: Time series of measured tN_r and tN_r scrubbed only (without interpolation) compared to the measured NH_2Cl by PTR-MS.

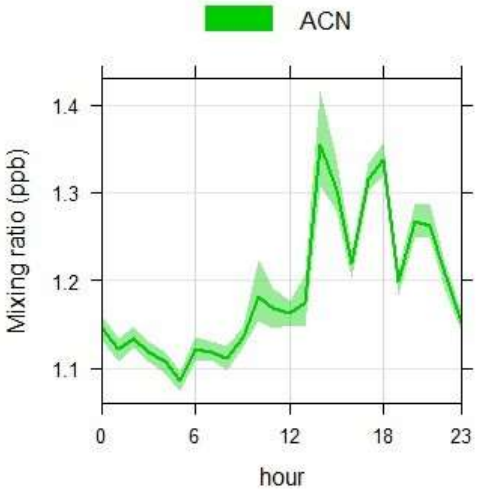

Fig S4: Mean diurnal trends in acetonitrile (ACN) as measured by the PTR-MS over the whole campaign[19].

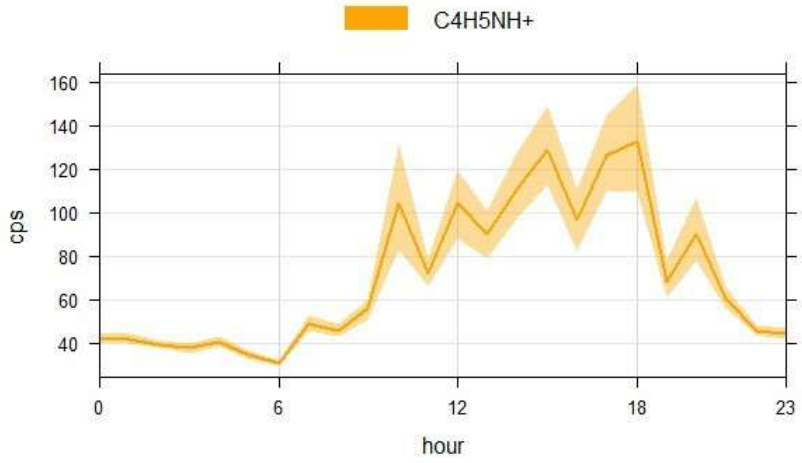

Fig S5: Mean diurnal trends in ion $C_4H_5NH^+$, nominally assigned to pyrrole (and isomers/fragments of higher molecular weight ions), as measured by the PTR-MS over the whole campaign.

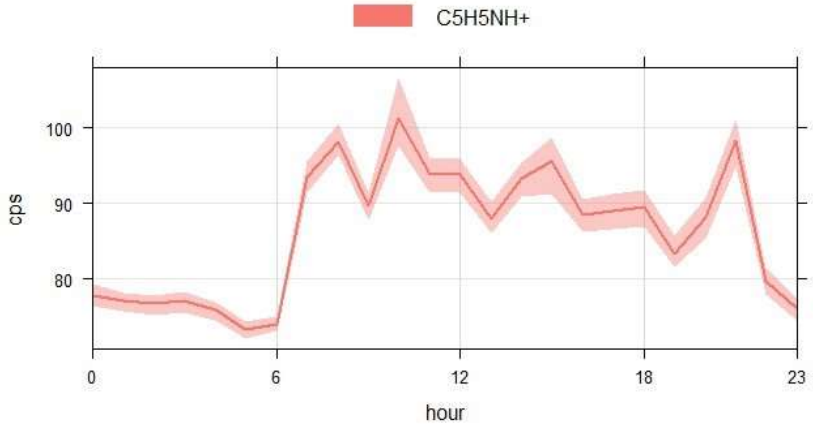

Fig S6: Mean diurnal trends in ion C_5H_5NH+, nominally assigned to pyridine (and isomers/fragments of higher molecular weight ions), as measured by the PTR-MS over the whole campaign.

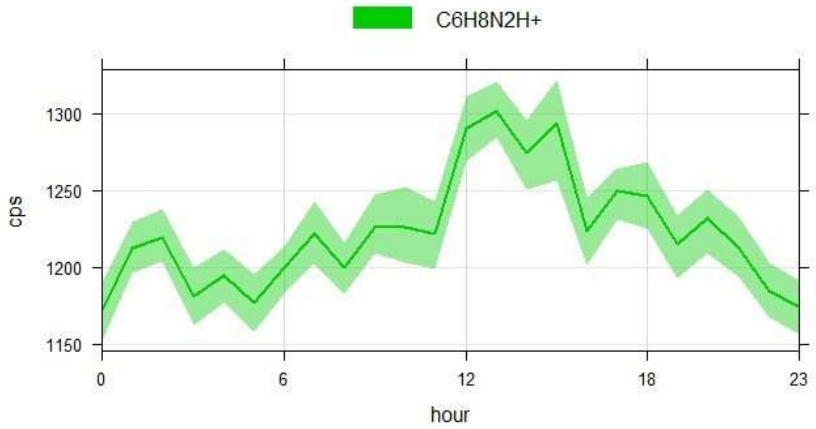

246

247 **Fig S7**: Mean diurnal trends in ion $C_6H_8N_2H+$, nominally assigned to alkylpyrazine (and
248 isomers/fragments of higher molecular weight ions), as measured by the PTR-MS over the
249 whole campaign.

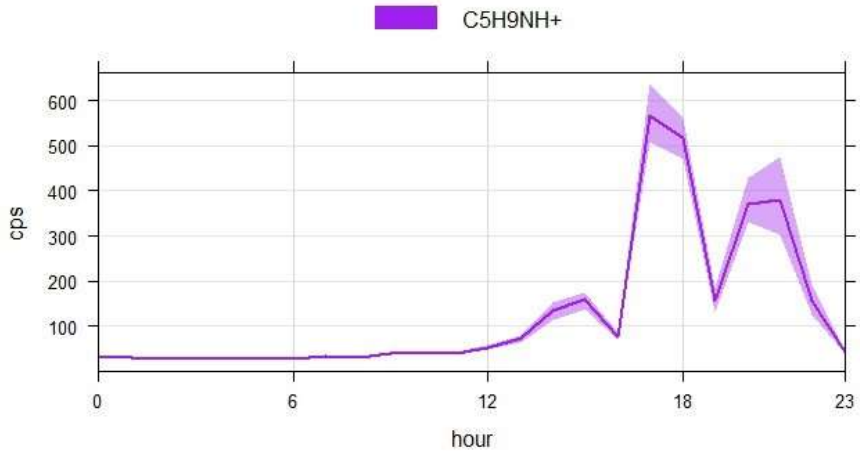

250

251 **Fig S8:** Mean diurnal trends in ion C_5H_9NH+, as measured by the PTR-MS over the whole
252 campaign.

253

254

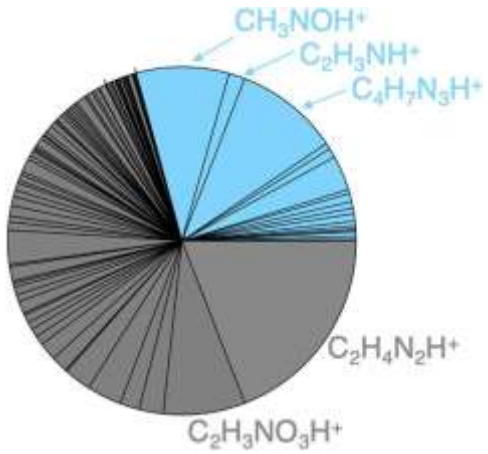

255

256 **Fig SG:** Pie chart of detected N-containing ions by PTR-MS during a chicken, salmon, and
257 vegetable cooking event (event #49-51). Blue coloured regions indicate ions detected during a
258 cooking oil + amino acid lab study[20].

259

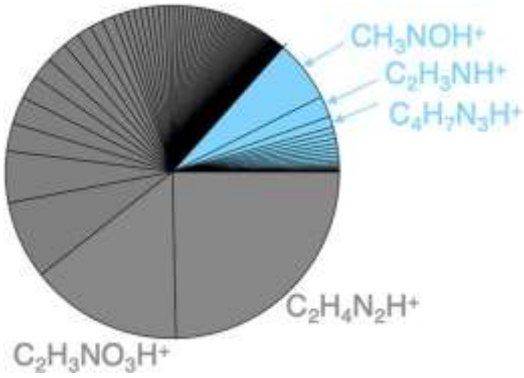

260

261 **Fig S10:** Pie chart of detected N-containing ions by PTR-MS during a pork and vegetable cooking
262 event (event #55). Blue coloured regions indicate ions detected during a cooking oil + amino acid
263 lab study[20].

264

265

S2. Reservoirs and partitioning fluxes of nitrous acid (HONO)

It is worth commenting that the observed very high NO_2 loss rates may reflect substantial heterogeneity in the kitchen originating from point sources near ventilation locations (i.e. stove under the range hood) diluting into the room volume beyond our inlets, while simultaneously being removed. Some portion of these higher values may also stem from our inability to capture the true S/V in this space, as we opted to use the common approximation method based on geometric room dimensions[21]. This does not capture the hidden spaces above the drop ceiling, behind walls, nor the porosity of room materials. Further, an in-use commercial kitchen has many added surfaces including storage racks, appliances, preparation equipment and tables, among many other supplies and apparatus. Therefore, the value of γ_{NO2} in this commercial kitchen could range from $1x10^{-6}$ up to 1.4×10^{-5}, with $2x10^{-6}$ reflective of a reasonable approximation based on the best direct comparison in the literature from a residential kitchen with a similar geometric S/V. In the following discussion, we present the results of simulations using this γ_{NO2} value and a nighttime unventilated ACR_{night} of 0.5 when the HVAC is off. In Table S2, we provide model outcomes at the upper ($\gamma_{NO2}=1.4x10^{-5}$; $ACR_{night}=0.1$) and lower ($\gamma_{NO2}=1x10^{-6}$; $ACR_{night}=1.0$) boundaries of the importance of NO_2 and our best estimate to compare the model to existing observations from the literature (Fig 6; $\gamma_{NO2}=2x10^{-6}$; $ACR_{night}=0.5$).

S2.1 Role of transport and photochemistry on HONO levels in the kitchen

The first source we consider is outdoor to indoor transport. While it may be possible for HONO produced outdoors at night to be brought indoors in the morning, kitchen activities and ventilation of this space start at 7 am, just following sunrise at 6 am, at which time substantial losses of HONO in the outdoor atmosphere by photolysis and planetary boundary layer mixing disrupting the nocturnal boundary layer would be expected. We were not able to measure HONO in the air supply duct and in the room during this work but can approximate its impact. During this brief period of the day ~50% of the HONO observed in the kitchen could be originating from outdoors if mixing ratios were on the order of 1 ppbv (2.5×10^{10} molec cm^{-3})[22]. Next, many studies have proposed indoor photochemical HONO production mechanisms[23–26], but the kitchen has no penetration of sunlight into its space, which negates their relevance to this indoor space. This makes the final option that surface reservoirs are the dominant and controlling driver of observed indoor HONO mixing ratios the most likely explanation, consistent with prior reports.

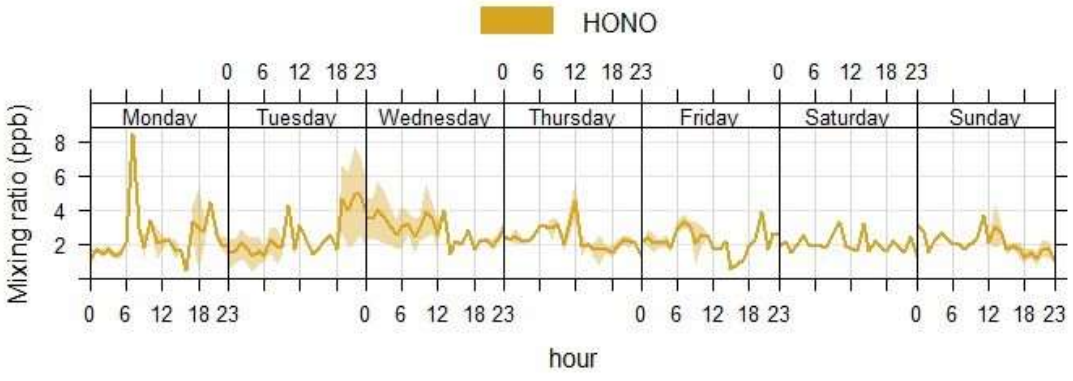

Fig S11: Mean diurnal trends of HONO as function of day of week.

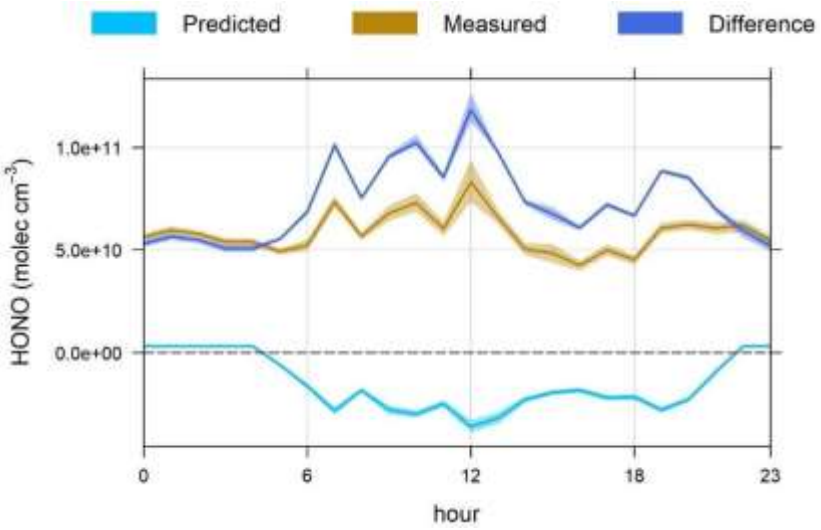

298

299 **Fig S12:** Mean diurnal trends in predicted HONO levels calculated from production of HONO
300 from NO_2 uptake on surfaces and loss by photolysis and ventilation compared to measured
301 HONO by day of week. The difference in predicted and measured HONO is also plotted. This is
302 using $\gamma_{NO2}=2x10^{-6}$; $ACR_{night}=0.5$ (See Table S2).

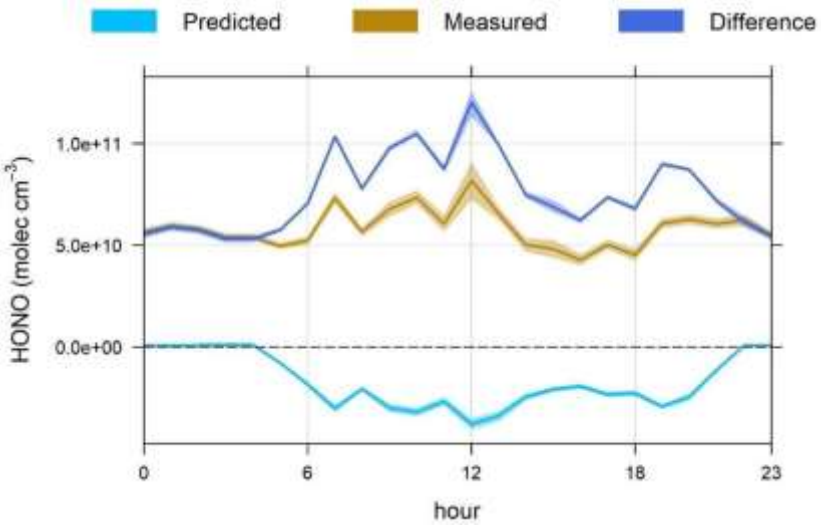

303

304 **Fig S13:** Mean diurnal trends in predicted HONO levels calculated from production of HONO
305 from NO_2 uptake on surfaces and loss by photolysis and ventilation compared to measured
306 HONO by day of week. The difference in predicted and measured HONO is also plotted. This is
307 using $\gamma_{NO2}=1x10^{-6}$; $ACR_{night}=1.0$ (See Table S2).

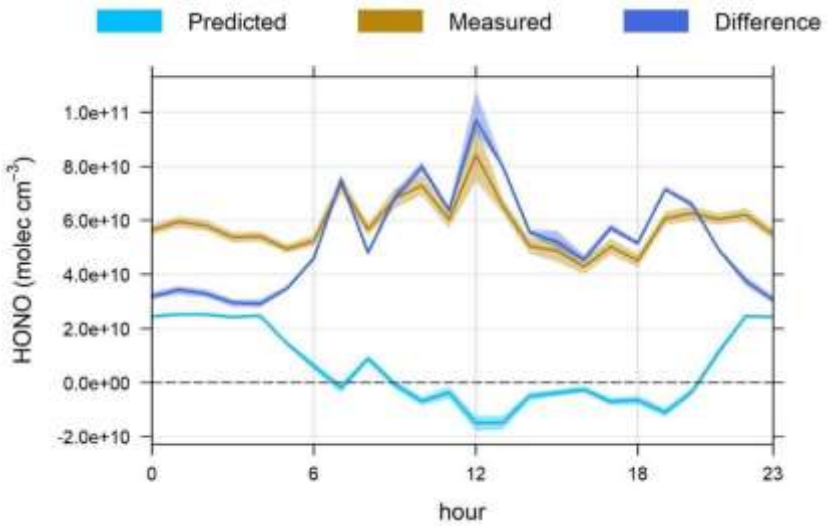

Fig S14: Mean diurnal trends in predicted HONO levels calculated from production of HONO from NO_2 uptake on surfaces and loss by photolysis and ventilation compared to measured HONO by day of week. The difference in predicted and measured HONO is also plotted. This is using γ_{NO2}=1.4x10^{-5}; ACR_{night}=0.1 (See Table S2).

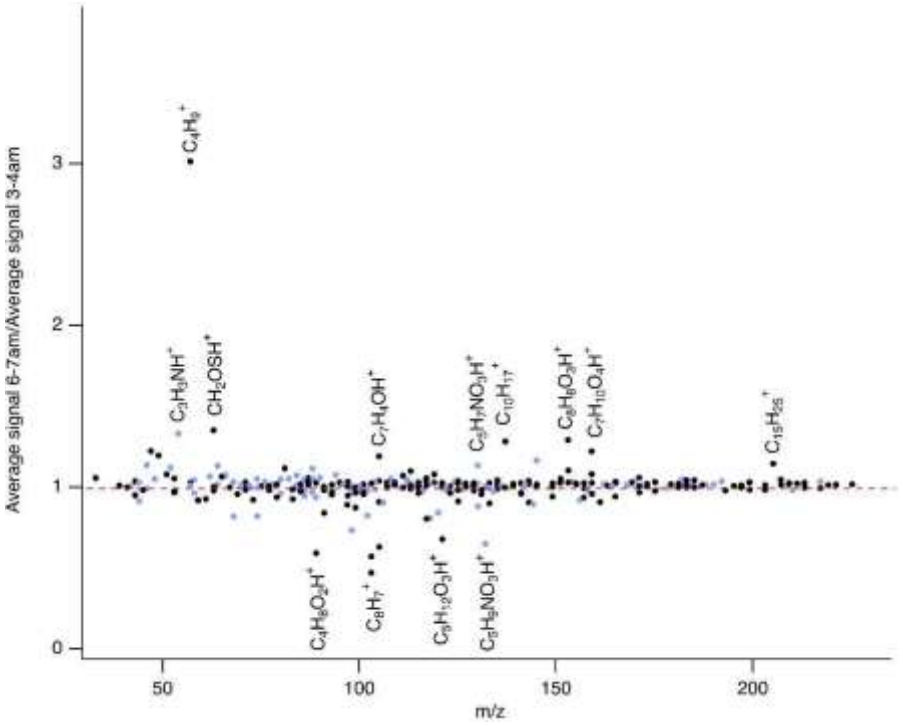

Fig S15: Mean PTR-MS ion signals averaged daily from 6-7 am (during ventilation ramp-up but prior to cooking/cleaning emissions) divided by mean ion signals averaged daily from 3-4 am (overnight, with no mechanical ventilation or emissions sources). The red dashed line shows a 1:1 ratio, indicating no change in signal with ventilation ramp up. Blue-shaded points represent nitrogen-containing ions.

References

1 Q. Liu and J. P. D. Abbatt, Liquid crystal display screens as a source for indoor volatile organic compounds, *Proc. Natl. Acad. Sci.*, 2021, **118**, e2105067118.

2 J. C. Ditto, L. R. Crilley, M. Lao, T. C. VandenBoer, J. P. D. Abbatt and A. W. H. Chan, Indoor and outdoor air quality impacts of cooking and cleaning emissions from a commercial kitchen, *Environ. Sci. Process. Impacts*, 2023, **25**, 964–979.

3 Y. Li, U. Pöschl and M. Shiraiwa, Molecular corridors and parameterizations of volatility in the chemical evolution of organic aerosols, *Atmos. Chem. Phys.*, 2016, **16**, 3327–3344.

4 B. Deming, D. Pagonis, X. Liu, D. Day, R. Talukdar, J. Krechmer, J. A. de Gouw, J. L. Jimenez and P. J. Ziemann, Measurements of Delays of Gas-Phase Compounds in a Wide Variety of Tubing Materials due to Gas-Wall Interactions, *Atmos. Meas. Tech. Discuss.*, 2019, 1–19.

5 D. Pagonis, K. Sekimoto and J. de Gouw, A Library of Proton-Transfer Reactions of H3O+ Ions Used for Trace Gas Detection, *J. Am. Soc. Mass Spectrom.*, 2019, **30**, 1330–1335.

6 D. Key, J. Stihle, J.-E. Petit, C. Bonnet, L. Depernon, O. Liu, S. Kennedy, R. Latimer, M. Burgoyne, D. Wanger, A. Webster, S. Casunuran, S. Hidalgo, M. Thomas, J. A. Moss and M. M. Baum, Integrated method for the measurement of trace nitrogenous atmospheric bases, *Atmos. Meas. Tech.*, 2011, **4**, 2795–2807.

7 W. Winberry Jr, T. Ellestad and B. Stevens, *DETERMINATION OF REACTIVE ACIDIC AND BASIC GASES AND STRONG ACIDITY OF ATMOSPHERIC FINE PARTICLES*, 1999.

8 L. Salehpoor and T. C. Vandenboer, A highly selective, sensitive, and accurate ion chromatographic method with a conductivity detection for quantitative analysis of alkylamines in the aerosol and gas phases, *Anal. Methods*.

9 D. B. Collins, R. F. Hems, S. Zhou, C. Wang, E. Grignon, M. Alavy, J. A. Siegel and J. P. D. Abbatt, Evidence for Gas-Surface Equilibrium Control of Indoor Nitrous Acid, *Environ. Sci. Technol.*, 2018, **52**, 12419–12427.

10 M. Mendez, N. Blond, D. Amedro, D. A. Hauglustaine, P. Blondeau, C. Afif, C. Fittschen and C. Schoemaecker, Assessment of indoor HONO formation mechanisms based on in situ measurements and modeling, *Indoor Air*, 2017, **27**, 443–451.

11 T. C. VandenBoer, M. Z. Markovic, J. E. Sanders, X. Ren, S. E. Pusede, E. C. Browne, R. C. Cohen, L. Zhang, J. Thomas and W. H. Brune, Evidence for a nitrous acid (HONO) reservoir at the ground surface in Bakersfield, CA, during CalNex 2010, *J. Geophys. Res. Atmos.*, 2014, **11G**, 9093–9106.

12 T. C. VandenBoer, C. J. Young, R. K. Talukdar, M. Z. Markovic, S. S. Brown, J. M. Roberts and J. G. Murphy, Nocturnal loss and daytime source of nitrous acid through reactive uptake and displacement, *Nat. Geosci.*, 2015, **8**, 55–60.

13 M. E. Monge, B. D'Anna and C. George, Nitrogen dioxide removal and nitrous acid formation on titanium oxide surfaces-an air quality remediation process?, *Phys. Chem. Chem. Phys.*, 2010, **12**, 8991–8998.

14 R. Ammar, M. E. Monge, C. George and B. D'Anna, Photoenhanced NO2 Loss on Simulated Urban Grime, *ChemPhysChem*, 2010, **11**, 3956–3961.

15 S. F. Kowal, S. R. Allen and T. F. Kahan, Wavelength-Resolved Photon Fluxes of Indoor Light Sources: Implications for HOx Production, *Environ. Sci. Technol.*, 2017, **51**, 10423–10430.

16 L. R. Crilley, M. Lao, L. Salehpoor and T. C. VandenBoer, Emerging investigator series: an instrument to measure and speciate the total reactive nitrogen budget indoors: description and field measurements, *Environ. Sci. Process. Impacts*, 2023.

17 K. Sekimoto, S.-M. Li, B. Yuan, A. Koss, M. Coggon, C. Warneke and J. de Gouw, Calculation of the sensitivity of proton-transfer-reaction mass spectrometry (PTR-MS) for organic trace gases using molecular properties, *Int. J. Mass Spectrom.*, 2017, **421**, 71–94.

18 L. J. Kramer, L. R. Crilley, T. J. Adams, S. M. Ball, F. D. Pope and W. J. Bloss, Nitrous acid (HONO) emissions under real-world driving conditions from vehicles in a UK road tunnel, *Atmos. Chem. Phys.*, 2020, **20**, 5231–5248.

19 W. D. Fahy, F. Wania and J. P. D. Abbatt, When Does Multiphase Chemistry Influence Indoor Chemical Fate?, *Environ. Sci. Technol.*, 2024, **58**, 4257–4267.

20 J. C. Ditto, J. P. D. Abbatt and A. W. H. Chan, Gas- and Particle-Phase Amide Emissions from Cooking: Mechanisms and Air Quality Impacts, *Environ. Sci. Technol.*, 2022, **56**, 7741–7750.

21 A. T. Hodgson, K. Y. Ming and B. C. Singer, *Quantifying object and material surface areas in residences*, Lawrence Berkeley National Lab.(LBNL), Berkeley, CA (United States), 2005.

22 C. L. Schiller, S. Locquiao, T. J. Johnson and G. W. Harris, Atmospheric measurements of HONO by tunable diode laser absorption spectroscopy, *J. Atmos. Chem.*, 2001, **40**, 275–293.

23 A. Depoorter, C. Kalalian, C. Emmelin, C. Lorentz and C. George, Indoor heterogeneous photochemistry of furfural drives emissions of nitrous acid, *Indoor Air*, 2021, **31**, 682–692.

24 J. Liu, H. Deng, P. S. J. Lakey, H. Jiang, M. Mekic, X. Wang, M. Shiraiwa and S. Gligorovski, Unexpectedly High Indoor HONO Concentrations Associated with Photochemical NO2 Transformation on Glass Windows, *Environ. Sci. Technol.*, 2020, **54**, 15680–15688.

25 S. Pandit, S. L. Mora Garcia and V. H. Grassian, HONO Production from Gypsum Surfaces Following Exposure to NO2 and HNO3: Roles of Relative Humidity and Light Source, *Environ. Sci. Technol.*, 2021, **55**, 9761–9772.

26 H. Schwartz-Narbonne, S. H. Jones and D. J. Donaldson, Indoor lighting releases gas phase nitrogen oxides from indoor painted surfaces, *Environ. Sci. Technol. Lett.*, 2019, **6**, 92–97.